Bulletin of the Seismological Society of America, Vol. 95, No. 4, pp. 1428–1446, August 2005, doi: 10.1785/0120040022

Strong Ground Motion in the Taipei Basin from the 1999 Chi-Chi, Taiwan, Earthquake

by Jon B. Fletcher and Kuo-Liang Wen

Abstract The Taipei basin, located in northwest Taiwan about 160 km from the epicenter of the Chi-Chi earthquake, is a shallow, triangular-shaped basin filled with low-velocity fluvial deposits. There is a strong velocity contrast across the basement interface of about 600 m/sec at a depth of about 600–700 m in the deeper section of the basin, suggesting that ground motion should be amplified at sites in the basin. In this article, the ground-motion recordings are analyzed to determine the effect of the basin both in terms of amplifications expected from a 1D model of the sediments in the basin and in terms of the 3D structure of the basin. Residuals determined for peak acceleration from attenuation curves are more positive (amplified) in the basin (average of 5.3 cm/sec^2 compared to -24.2 cm/sec^2 for those stations outside the basin and between 75 and 110 km from the surface projection of the faulted area, a 40% increase in peak ground acceleration). Residuals for peak velocity are also significantly more positive at stations in the basin (31.8 cm/sec compared to 20.0 cm/sec out). The correlation of peak motion with depth to basement, while minor in peak acceleration, is stronger in the peak velocities. Record sections of ground motion from stations in and around the Taipei basin show that the largest long-period arrival, which is coherent across the region, is strongest on the vertical component and has a period of about 10–12 sec. This phase appears to be a Rayleigh wave, probably associated with rupture at the north end of the Chelungpu fault. Records of strong motion from stations in and near the basin have an additional, higher frequency signal: nearest the deepest point in the basin, the signal is characterized by frequencies of about 0.3 – 0.4 Hz. These frequencies are close to simple predictions using horizontal layers and the velocity structure of the basin. Polarizations of the *S* wave are mostly coherent across the array, although there are significant differences along the northwest edge that may indicate large strains across that edge of the basin. The length of each record after the main *S* wave are all longer at basin stations compared to those outside. This increase in duration of ground shaking is probably caused by amplification of ground motion at basin stations, although coda Q (0.67 – 1.30 Hz) is slightly larger inside the basin compared to those at local stations outside the basin. Durations correlate with depth to basement. These motions are in the range that can induce damage in buildings and may have contributed to the structural collapse of multistory buildings in the Taipei basin.

Introduction

The Chi-Chi earthquake of 20 September 1999 ruptured a 100-km segment of the Chelungpu fault along a north–south line on the western edge of the central mountains of Taiwan (Shin and Teng, 2001). Its magnitude of 7.6 makes it the largest Taiwanese earthquake of the twentieth century. Approximately 2,300 people were killed and 10,000 people were injured (Shin *et al.*, 2000). Similar to the Northridge earthquake (M_W 6.7, 17 January 1994) that struck the Los Angeles, California, area, basins in urban areas near these earthquakes may have amplified the ground motion within certain frequency bands and contributed to the loss of life and structural damage.

Fortunately, with the installation of an extensive network of strong-motion instruments by the Central Weather Bureau of Taiwan (Shin *et al.*, 2000), we may be able to more accurately determine the response of basins to strong shaking and reduce the future loss of life. The Central Weather Bureau's array consists of at least 650 strong-

motion instruments deployed in the free field as well as 55 arrays of strong-motion sensors to study the response of engineered structures to strong shaking (Shin *et al.*, 2000). Of particular interest here are the 50 or so stations deployed in or near the Taipei basin (see Fig. 1). This number of instruments makes it possible to see areal trends, which will allow identification of the particular characteristics associated with the seismic waves traveling through the basins. Once we identify these waves, we can then correlate their characteristics with parameters that describe the basin and predict their behavior with 1D models or visualize the response of the basin with a full 3D simulation.

Data

The recordings of strong ground motion from the network of about 50 accelerographs that lie in the Taipei basin and surrounding area comprise an important data set for studying the response of basins. These instruments remain on scale for large damaging shocks (they typically clip at 2*g*, Shin *et al.*, 2000), and have a response that is flat-to-ground acceleration from zero to the natural frequency of the sensor (about 50 Hz). Most run at 200 samples/sec with 16-bit resolution. For many of these stations, data can be telemetered back to a central recording site in near real time using telephone lines. Preliminary data were published by Lee *et al.* (1999).

Geography and Geology of the Taipei Basin

The Taipei basin sits at the northwestern edge of the island of Taiwan (see Fig. 1). It is triangular in shape with each side about 20 km long and its apex pointing toward the coast. It is deepest near the western edge, where the depth to basement is about 600–700 m (Wen and Peng, 1998). On the eastern side, the interface with the basement is flatter, with a more constant depth of around 100–200 m. The geometry of the western edge of the basin is probably controlled by the Shanchiao fault (Bonilla, 1975). In the basin, Quaternary-aged silty sands, clays, and conglomerates overlie a Tertiary basement. Table 1 gives a brief description of the geologic formations in the basin and the depth interval for each. Data for V_P, V_S, and depth to the formation come from two sources. Wen and Peng (1998) give a table of velocities and formation thicknesses based on borehole and reflection surveys (Wang *et al.*, 1996) and are listed in the third and fifth columns in Table 1. More recently, however, logs from boreholes (Lin and Chen, 2001) show that the basin is almost 700 m deep near the western edge, and these estimates of depth to the various horizons are used in the following estimates of the 1D response of the deep part of the basin. Lin and Chen (2001) did not break the Sungshan Formation into the three subunits, and these velocities are estimated to be slightly higher than the velocities given by Wen and Peng (1998) to coincide with the higher velocity given for the Chingmei formation by Lin and Chen, 2001).

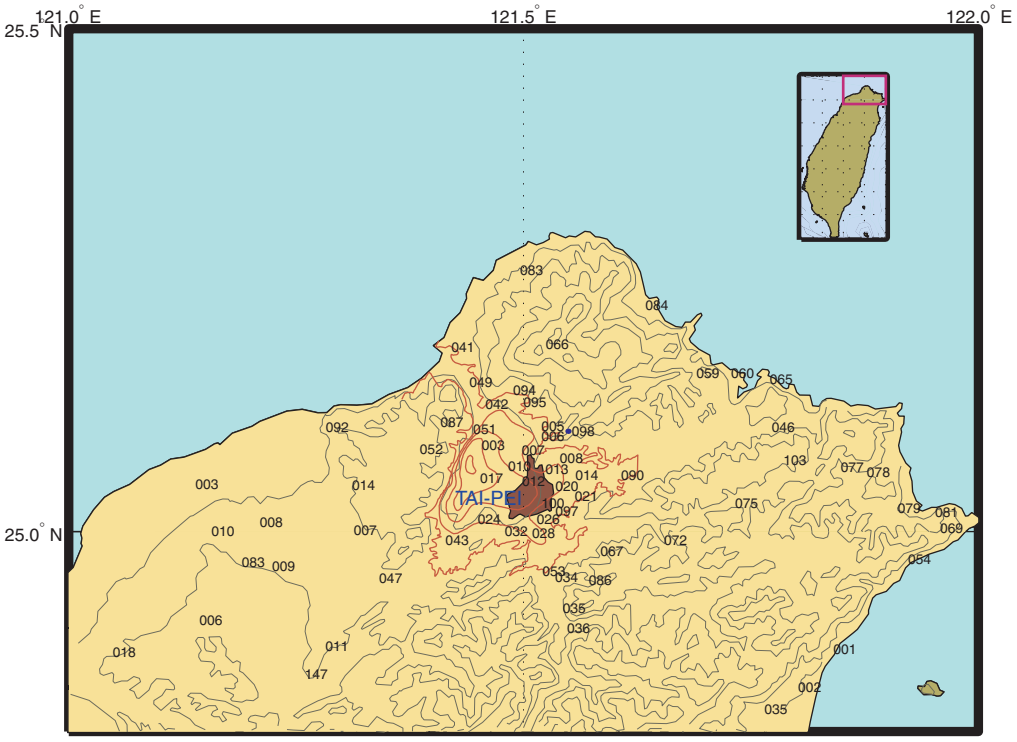

Figure 1. Map of stations in and around the Taipei basin. Numbers identify each station. Contours are depth to basement in 100-m intervals, from Wen and Peng (1998).

Table 1
Geologic and Velocity Structure of Taipei Basin

Formation	Description	Depth to Top of Formation Deep Section	Depth from Boreholes, Wk-1E	Depth of Southeast (shallow) Section (m)	V_P (m/sec)	V_S (m/sec)
Sungshan	Alternating beds of silty clay and sand	0	0	0	450	170
		20	25†	15	1500	230
		50	55†	35	1600	340
Chingmei	Conglomerate	100	110	50	1800	450
Wuku*	Clayey sand with	160	151	100	2000	600
Panchiao*	comglomerate	320	300	200	2200	650
Basement		400	679	250	3000	1200

After Wen and Peng (1998) and from Lin and Chen (2001).
*These formations are subunits of the Hsinchuang Formation.
†Estimated.

Shear-wave velocities range from 170 to 650 m/sec in the basin and then jump to 1200 m/sec in the basement (Wen and Peng, 1998). *P*-wave velocities range from 450 to 3000 m/sec in the basin (Wen *et al.*, 1995; Wen and Peng, 1998). With a shear-wave velocity contrast across the basement interface of approximately 600 m/sec, we would expect the Taipei basin to trap and amplify seismic waves.

Chung and Shin (1999) recorded surface waves across the northern end of Taiwan from an earthquake near the Ilam basin on the northeastern shore. Inversion of Love waves (the event had a left-lateral strike-slip mechanism) yielded a velocity model for the upper crust in the region of the Taipei basin. Although their ray paths transect the basin, they cannot resolve the velocities in the basin because they can only resolve frequencies lower than 0.5 Hz. Their basement velocities, however, are similar to those reported from Wen and Peng (1998) of about 1200 m/sec.

Peak Motion

Peak motion from most large earthquakes has been analyzed as functions of magnitude and distance to determine prediction relations for damaging ground motions (Joyner and Boore, 1981; Boore *et al.*, 1997; Campbell, 1997; Youngs *et al.*; 1997, etc.). From Boore *et al.* (1997)

$$\ln a = b_1 + b_2(M - 6) + b_3(M - 6)^2 + b_5 \ln r + b_v \ln \frac{v_s}{v_a},$$

where a is either pseudoacceleration response spectra or peak acceleration, b_i are coefficients determined by regression on recorded strong-motion data and V_s/V_a, the ratio of the shear velocity in the upper 30 m to a regressed value, is a site amplification term. For peak acceleration, Boore *et al.* (1997) found that b_3 was zero, and b_5, correcting for distance, was -0.778. Figure 2 shows the peak horizontal accelerations from the Chi-Chi earthquake compared to the Boore *et al.* (1997) model (see also, Boore, 2001). A site term is set to "rock" or, equivalently, the local near-surface velocity is presumed to be 620 m/sec (setting this value to "soil" does not change the overall appearance of the plot and increases the root mean square (rms) of the residuals from -96.7 to -154.7 cm/sec^2). Consequently, we are not correcting for the amplification of the site-specific, low-velocity sediments in the basin even though there is a correction term in the attenuation formula because we do not have the necessary geotechnical information at the strong-motion sites in the Taipei basin. Boore *et al.* (1997) calculates distance from the nearest point on the surface projection of the fault plane. The fault plane used here was estimated from Figure 1 of Boore (2001). It is apparent that although there is abundant scatter, particularly at the shorter distances, the stations in and around the Taipei Basin (dots) have peak accelerations that are within the scatter of the other stations, but tend to be higher. The mean of the residuals is 5.3 cm/sec^2 for stations in the basin compared to -24.2 cm/sec^2 for stations outside the basin beyond 75 but less than 110 km, which brackets the distance from the fault plane of the basin stations. A Student's *t* test, which tests if two means are from the same parent distribution, shows that these means are not from the same distribution and are significantly different. This represents a 40% increase in ground shaking. There is also a contrast for peak velocity (Figure 3, using Joyner and Boore, 1988) when comparing residuals inside and outside the Taipei basin. Residuals of peak velocities in the basin average 31.8 cm/sec versus an average of 20.0 cm/sec for stations within the previous distance range, and these residuals for peak velocity are significantly different according to Student's *t* test and represent an average amplification of about 37%.

Correlation with Depth to Basement

Although it is common to observe amplification at stations located in basins, it is important to characterize these amplifications with respect to the shape and velocity structure of the basin. Figures 4 (residuals for peak acceleration)

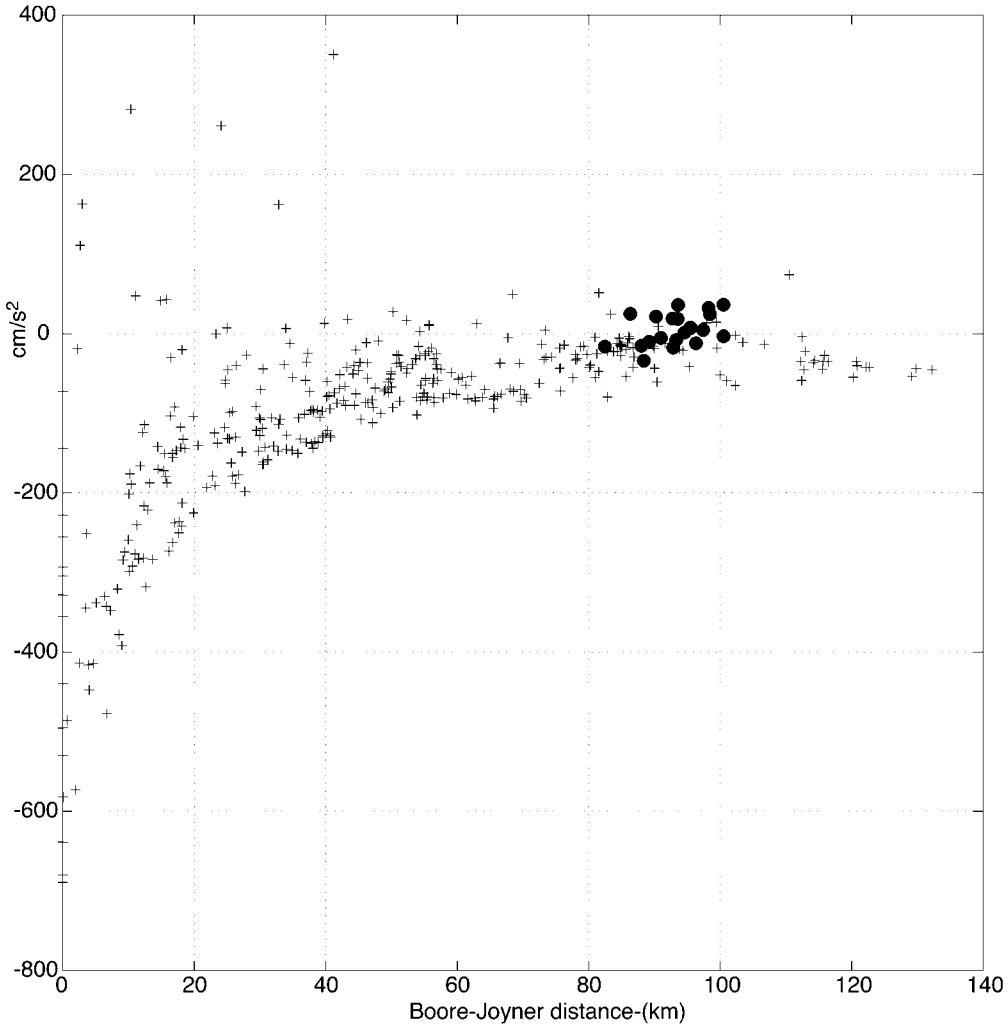

Figure 2. Residuals of peak horizontal accelerations with respect to the prediction of Boore *et al.* (1997). Dots are those in the Taipei basin. Note that most residuals have a value less than zero, which means that for that value the prediction was greater than the observation.

and 5 (residuals for peak velocity) show the regression of the residuals from the previous discussion with respect to depth to basement. Depth at each station is estimated from contours of depth to basement from Wen and Peng (1998). Figure 4 shows that although the residuals show an upward slope with respect to depth, the positive slope is not large and may not be different from zero. In Figure 5, though, we see that the residuals for peak velocities correlate with depth to basement, and the coefficient of 0.05 is significant. Further, this coefficient is considerably larger than that found for the Los Angeles basins of about (5–11) $\times$ 10^{-5} (Field, 2000). That the amplification versus depth is higher for the Taipei basin than it is for the Los Angeles basins is expected because the amplification is controlled mostly by the impedance contrast across the basement interface (Aki and Richards, 2002) and not the depth to basement. Consequently, the slope will be higher for shallower basins given the same impedance contrast at the basement interface.

Source and Basin Excitation

Velocity time series are plotted in Figure 6 versus epicentral distance. In order to plot each seismogram on a single graph, the timing at each station had to be calibrated against a single time standard as timekeeping was inconsistent across the array of strong-motion stations. For these data, the closest station was used as a master and cross-correlated against the other strong-motion records. The main phase used in the cross-correlation was the large 10 12-s pulse on the vertical (Fig. 6). These relative delay times were then fit by least squares to a best-fitting plane wave to determine clock corrections. This procedure also found apparent polarity reversals as the peak in the cross-correlation function will be negative if one of the traces is reversed relative to the master. Clock corrections were determined for the largest phase on the vertical component because coherence was high across all stations with coefficients better than 0.85 in most

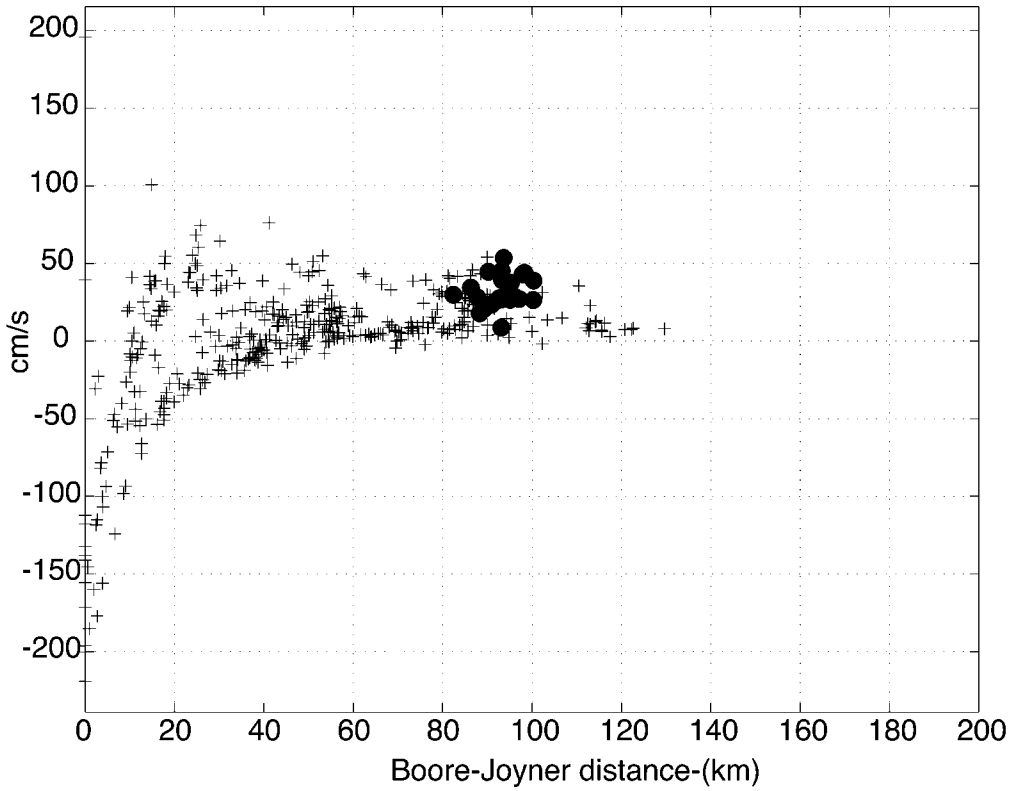

Figure 3. Residuals of peak horizontal velocity with respect to the prediction of Joyner and Boore (1988). Dots are those in the Taipei basin. Note that most residuals have a value greater than zero, which means that for that value the prediction was less than the observation.

cases (mean = 0.9). Coefficients were substantially lower at 0.5–0.8 for the horizontals (for the north component, mean = 0.7) with many peaks that were hard to discern above the background. On the vertical, the largest phase is a long-period arrival (e.g., centered at 150 sec at TAP081, Fig. 6) with a period of about 10 sec. It arrives after other high-frequency arrivals and is probably a Rayleigh wave created by the large displacements at the north end of the fault (Chi *et al.*, 2001; Wu *et al.*, 2001, etc.) with its travel time encompassing the time for the rupture front to travel from the source to the north end of the fault and surface-wave propagation from there to the north end of the island. The best-fitting plane wave had a velocity of 1.86 km/sec, which is similar to that reported for Love waves for the north end of the island (Chung and Shin, 1999). At stations that are in the Taipei basin, traces have an oscillation with a higher frequency (0.5 to 2 Hz), which typically lasts several tens of seconds after the *S* wave. It is easiest to see by comparing the coda part of the records on the transverse component (Fig. 8).

In Figures 9 and 10, we can see the particular frequencies associated with these waves. To visualize these peaks, we apply a Fourier transform to each velocity time series in Figure 6 or 7 and smooth with a 7-point running mean filter. The depth versus Fourier spectra field is then contoured. The source (Rayleigh) excitation, with a 10-s period, is the strongest peak on the vertical and compressed near the origin on the linear-frequency axis. Stations in the deep part of the basin such as 003 and 017 (depths of 313 and 373 m, respectively) have strong peaks at about 0.3 to 0.4 Hz (vertical) and also at frequencies of around 0.8–0.1 Hz (light blue in Fig. 10). Other stations, such as 020 (depth 132 m, Fig. 9) in the shallower part of the basin, have peaks at frequencies of about 0.7 Hz (light blue in Fig. 9).

We model the 1D response of the basin using the Haskell (1953) matrix method as implemented by Joyner *et al.* (1976). This method assumes incoming body waves and computes the response versus angle of incidence by using the boundary conditions at each flat interface. Taipei basin is approximately 150 km from the hypocenter, so body waves reach the lower crust and are refracted back to the surface at steep angles. Consequently, the Haskell approach seems appropriate for modeling the response of the basin to incoming body waves, but does not include effects caused by the 3D structure of the basin. Both the *SV* and *SH* responses of the deep section of the basin are shown in Figure 11a. The *SH* response is more stable, with the frequency of the peaks not changing very much as the angle of incidence

(*Text continues on page 1440.*)

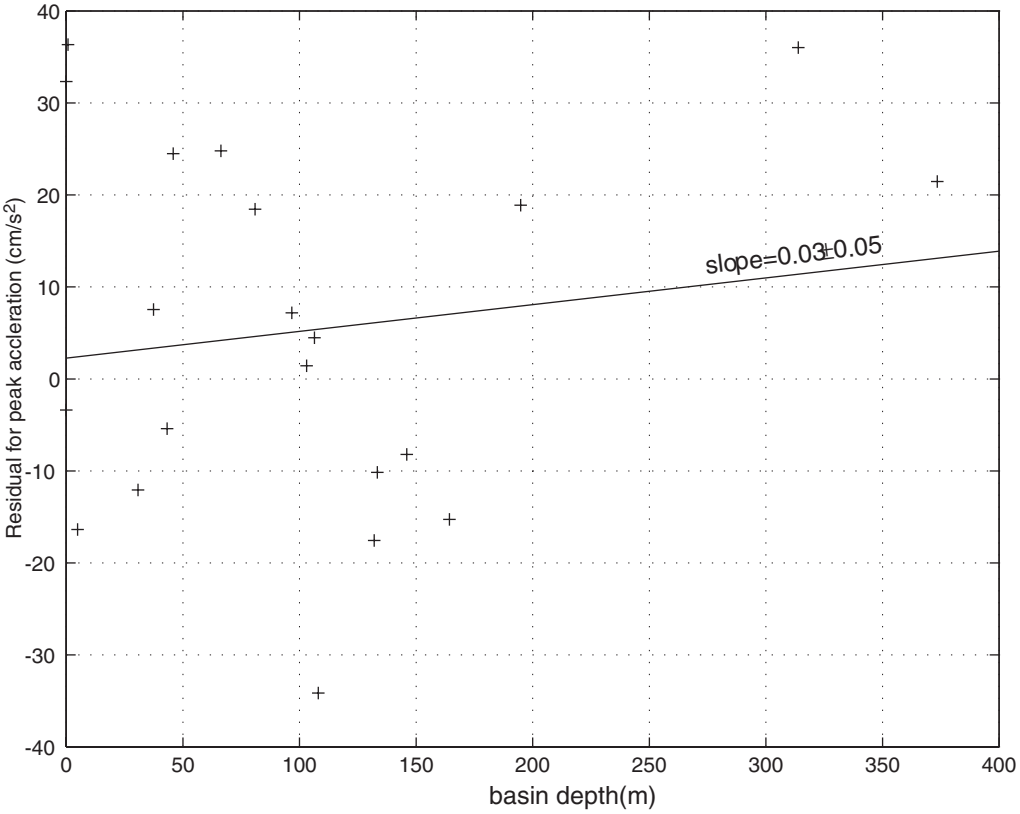

Figure 4. Residual of peak acceleration versus depth to basement in the Taipei basin. The value of slope is not significant as indicated by its error.

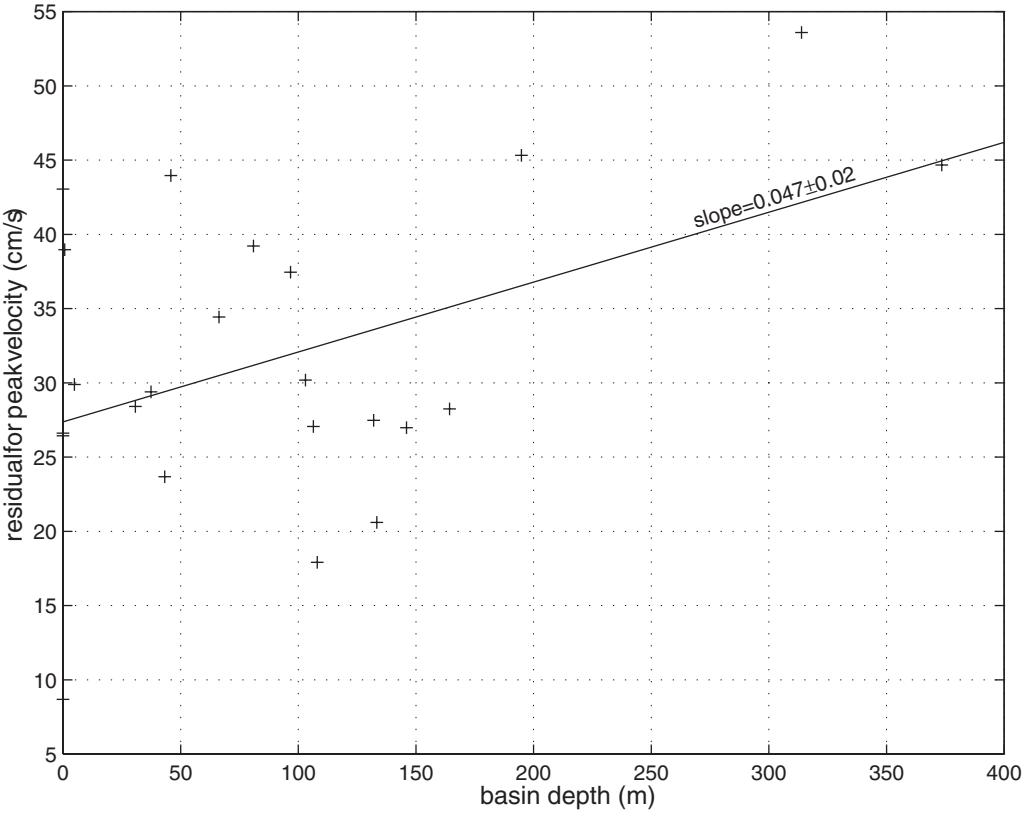

Figure 5. Residual of peak velocity versus depth to basement in the Taipei basin.

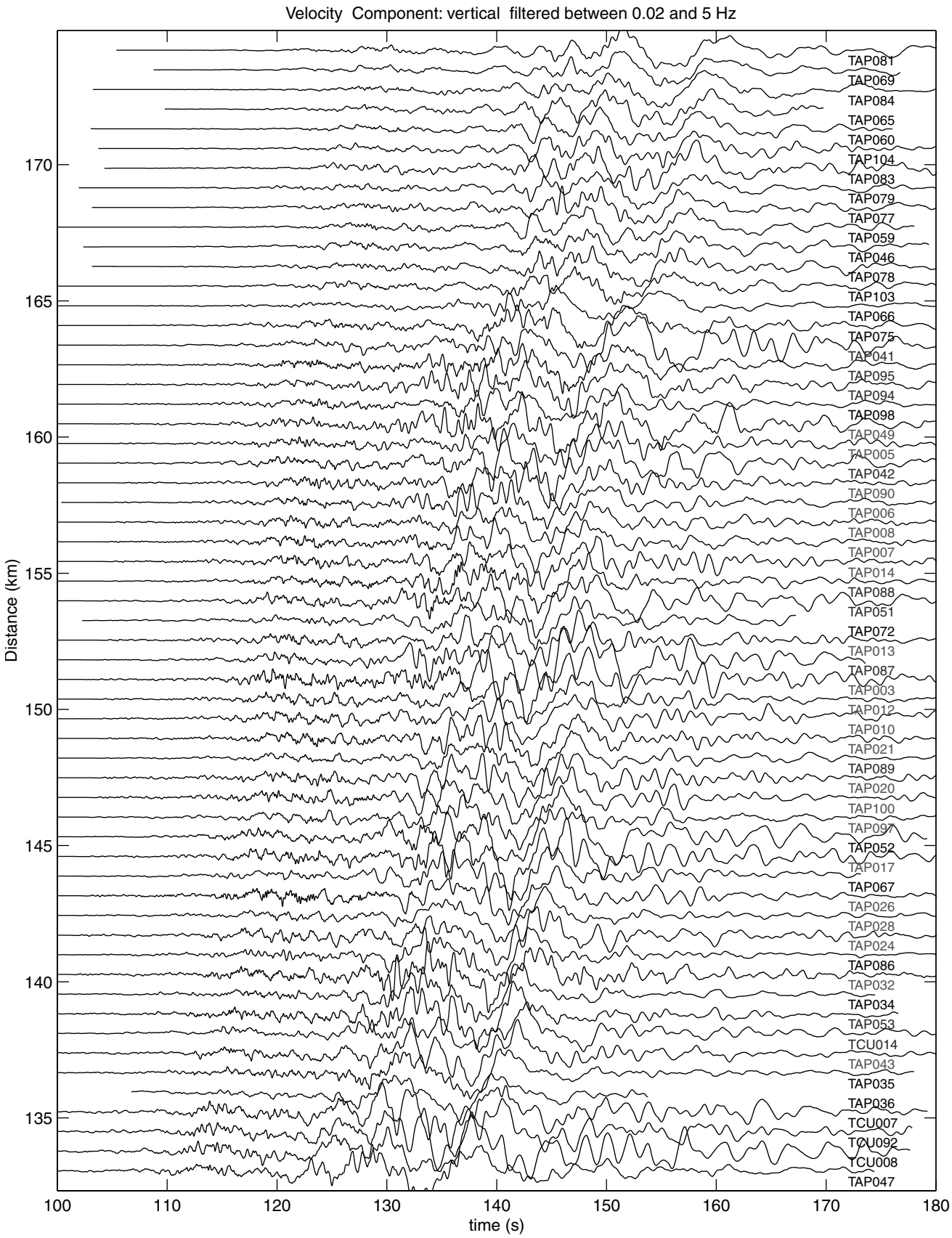

Figure 6. Vertical component of velocity for the stations near the northwest end of Taiwan. Note large phase with a period of about 10 sec, which arrives on most records between 130 and 160 sec. Each trace is individually scaled. Station names are given on the right. Distances are approximate to allow the best image for each trace.

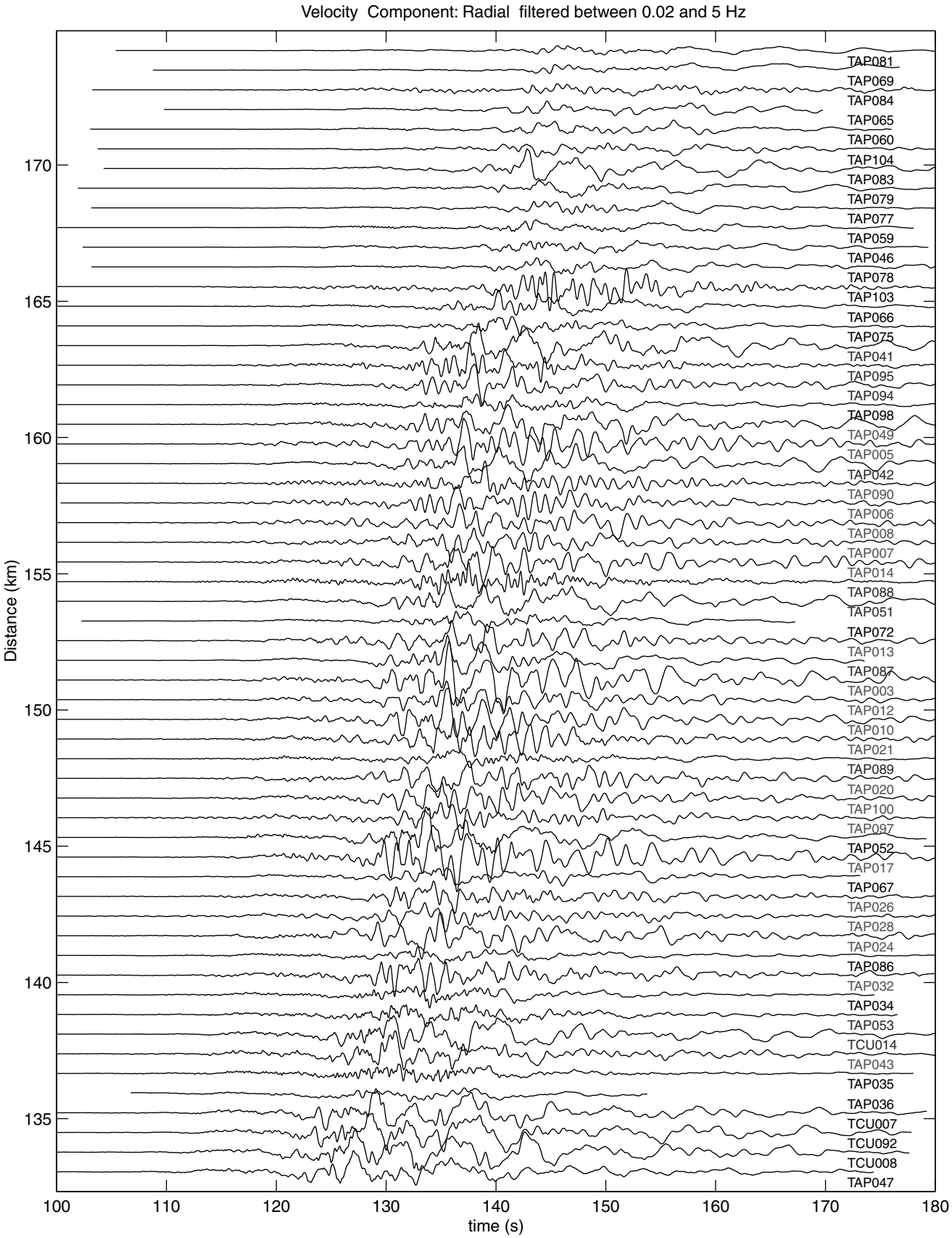

Figure 7. Radial component of velocity for the stations near the northwest end of Taiwan.

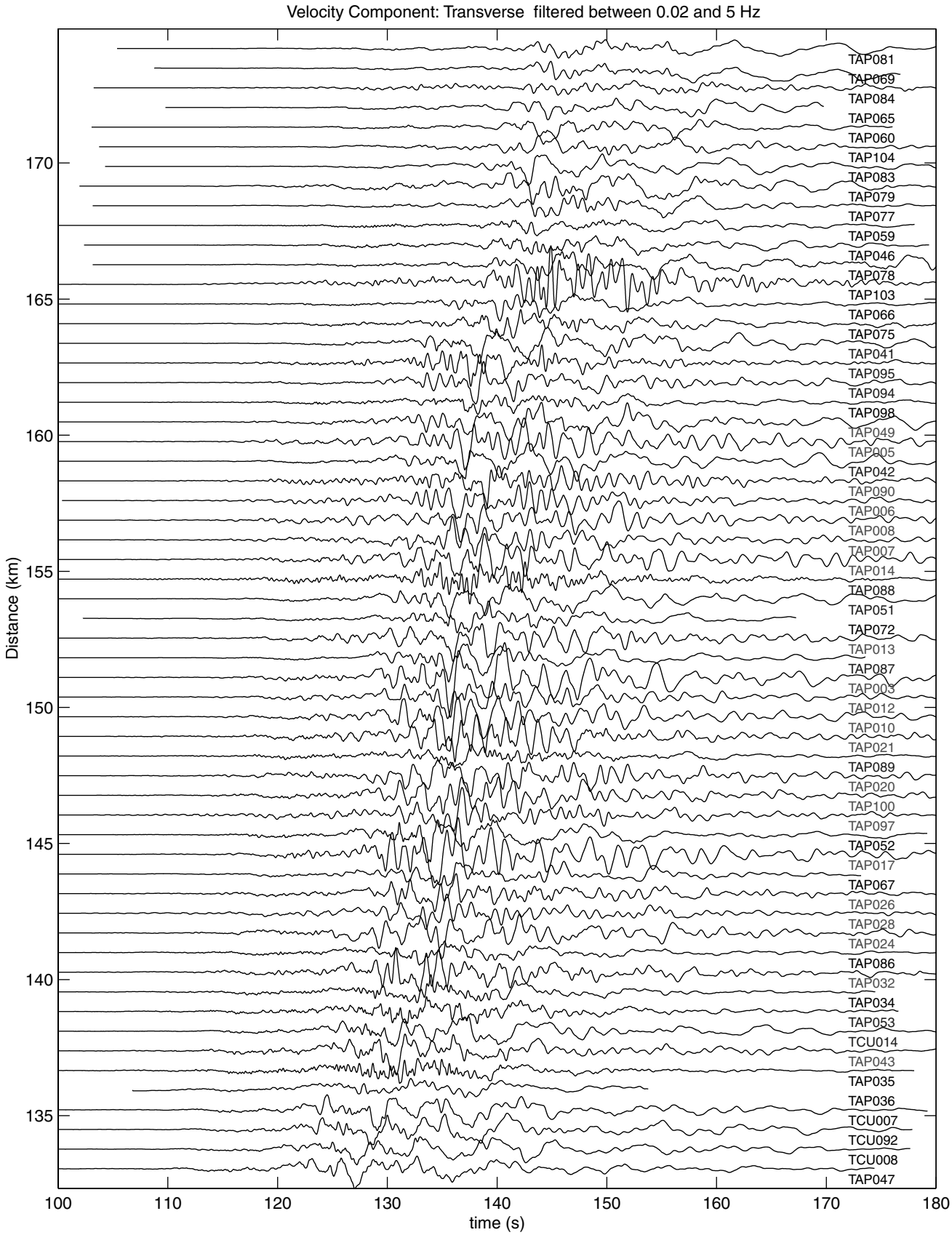

Figure 8. Transverse component of velocity for the stations near the northwest end of Taiwan.

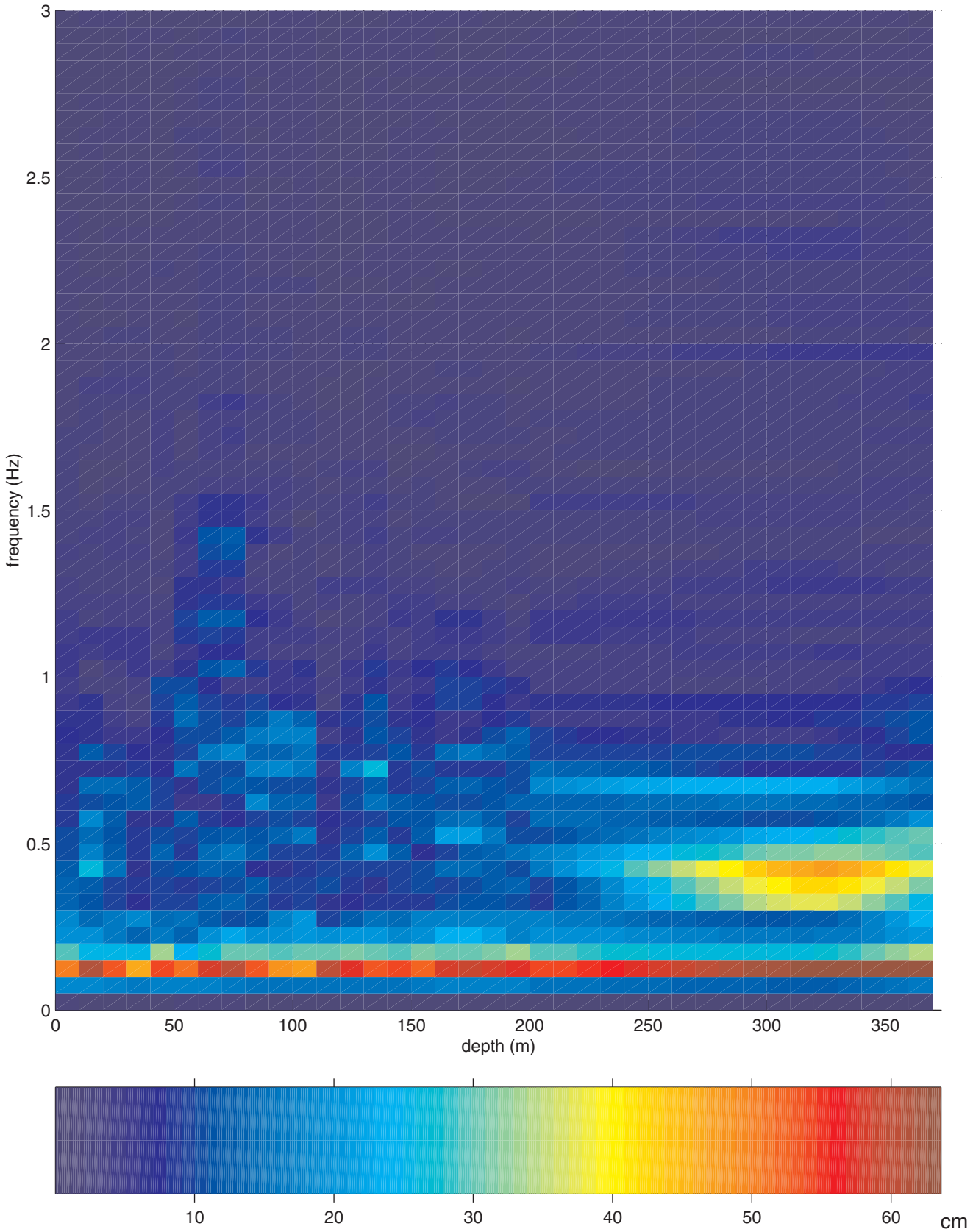

Figure 9. Contoured Fourier transform of data in Figure 5 after a 7-point running-mean filter. Note large peak near origin, which is caused by the large 10-sec phase.

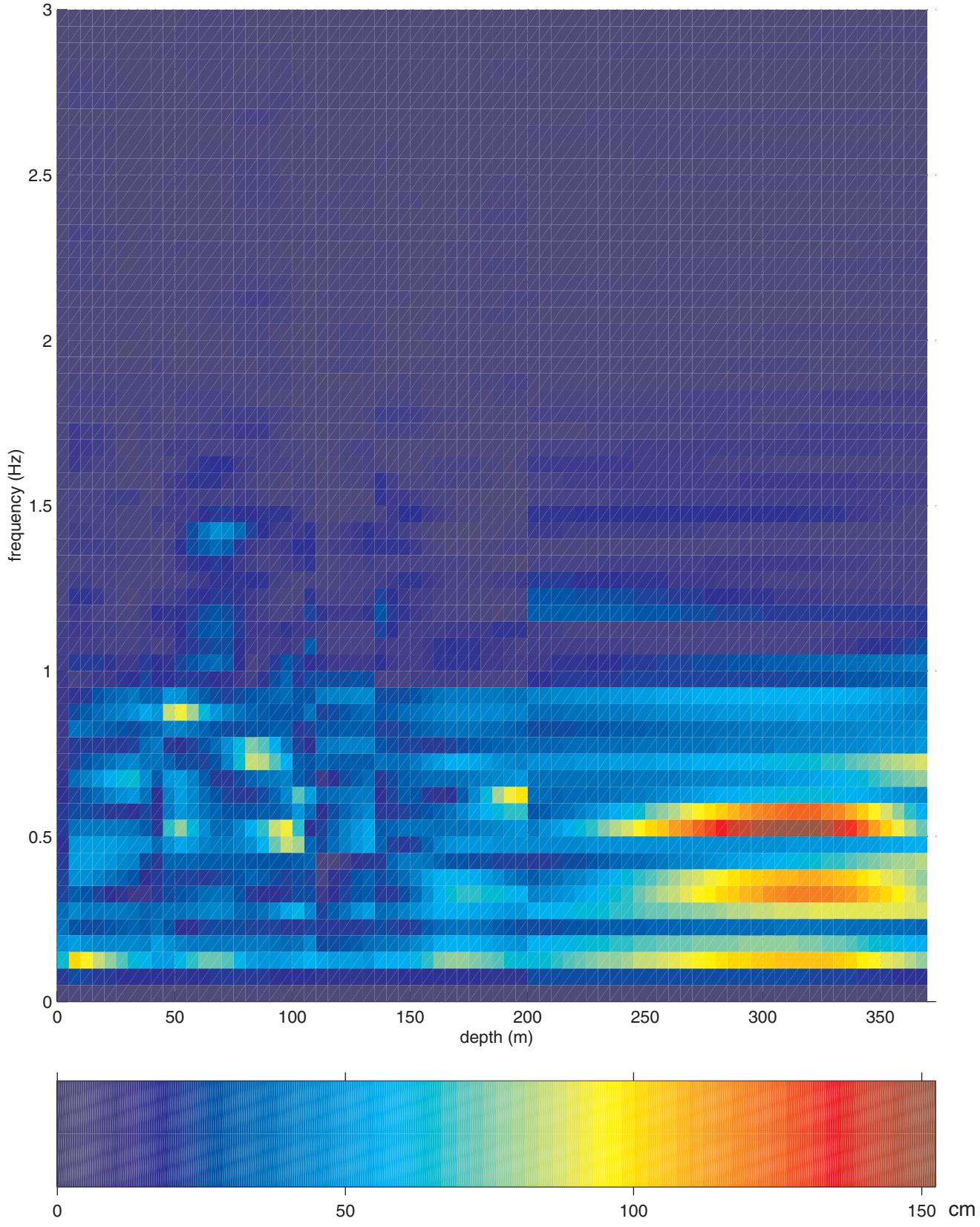

Figure 10. Similar to Figure 8, but for the radial component.

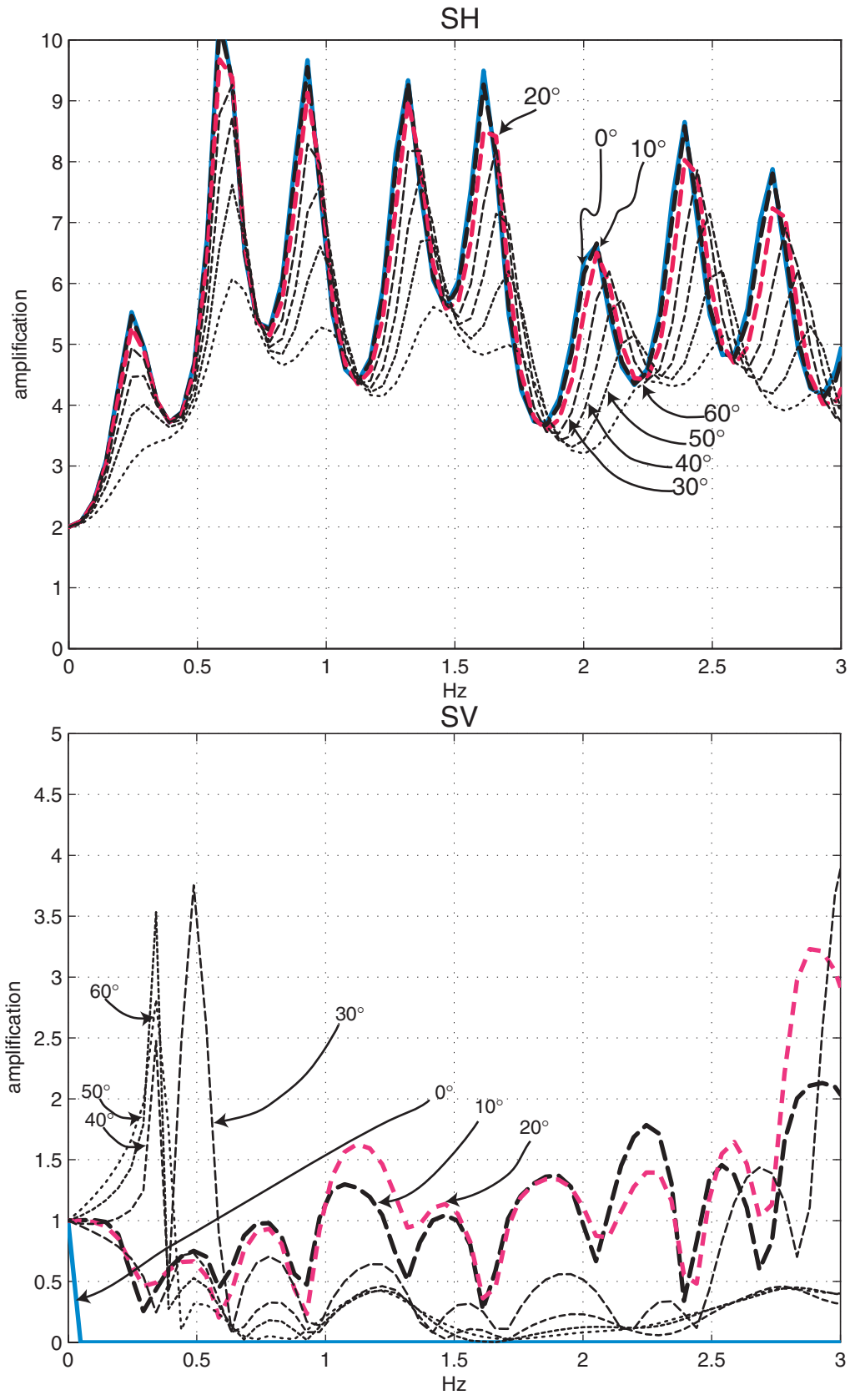

Figure 11. Response of 1D deep basin structure as a function of angle of incidence. Model is the same as the deep model in Table 1. The horizontal response to *SH* input is given in the top figure. The vertical response to an *SV* input motion is given in the bottom figure. Response determined using the method of Haskell (1953) as implemented by Joyner *et al.* (1976). (*continued*)

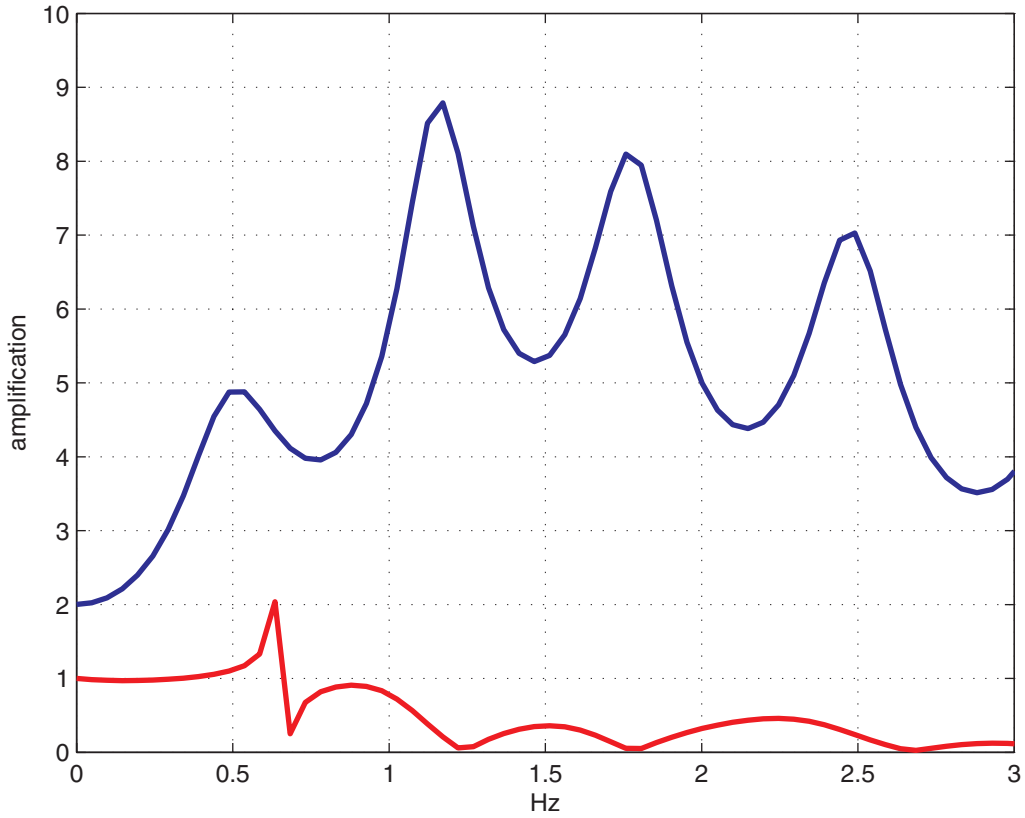

Figure 11 (*continued*). Predictions of site response for 1D velocity model of the southeast profile of the Taipei Basin at incident angle of 40°. Response is determined for both *SV* and *SH*.

changes from vertical to more horizontal. However, the peaks show less amplification as the rays move from vertical. The *SV* response, in contrast, changes rapidly as the angle of incidence moves from vertical to more horizontal. In fact, at near-vertical incidence, the response has no large peaks below 3 Hz, which we would expect for an *SV*-polarized wave on the vertical. However, modest peaks are found at frequencies of 0.3–0.5 Hz at incident angles of 30° or greater. Figure 11b shows the response of the southeast profile of Table 1 (Q is arbitrarily varied from a value of 40 at the surface to 90 at a depth of 300 m). The peak in the *SV* response at 0.6 Hz is close to the frequency of the peak seen in the contoured frequency plot for stations that are situated over the intermediate part of the basin on the radial component (Figure 10). Peaks at higher frequencies in the *SH* response such as at 1.2 Hz are not obvious in the spectra at these stations. One of the most apparent differences in the theoretical calculations between the *SH* and *SV* responses is that the amplification of peaks is much lower in the *SV* response when compared to the *SH* response, which has peaks approaching 9 in Figure 11a. The amplification in the peak velocity and peak acceleration at stations in the Taipei basin are more in agreement with the smaller amplifications found in the *SV* response.

Polarizations

Polarizations at four different times are plotted in Figure 12 to show the effect of the basin on the azimuth of the vector velocity. Each vector in Figure 12 was formed from the horizontal components taking into account known polarity reversals (Lee *et al.*, 1999). The initial *P* wave arrives at an absolute time of 100 sec on the record for Tap047 (Fig. 6), and another *P* wave probably arrives at about 110 sec from another part of the fault, probably the asperity at the north end. The first *S* wave arrives shortly after at about 120 sec. Polarizations in Figure 12a are plotted just before the main shear energy arrives, and coherence is seen in the eastern part of the Taipei basin. Note that polarizations are in opposite directions across the northwest boundary of the basin. About 5 sec later (Fig. 12b) in the largest part of the record, the shear wave at the eastern stations have a southeast azimuth, and stations near the middle part of the basin have northwesterly azimuths. Again, there are sharp contrasts across at the northwest basin boundary. For instance the azimuth at station 003 is almost directly opposite to that of the station just on the other side of the boundary to the basin (Figure 12b). In Figure 12c, one-half cycle later than Figure 12b, the pattern is similar to Figure 12b with the eastern group having opposite polarities to that of the group in the

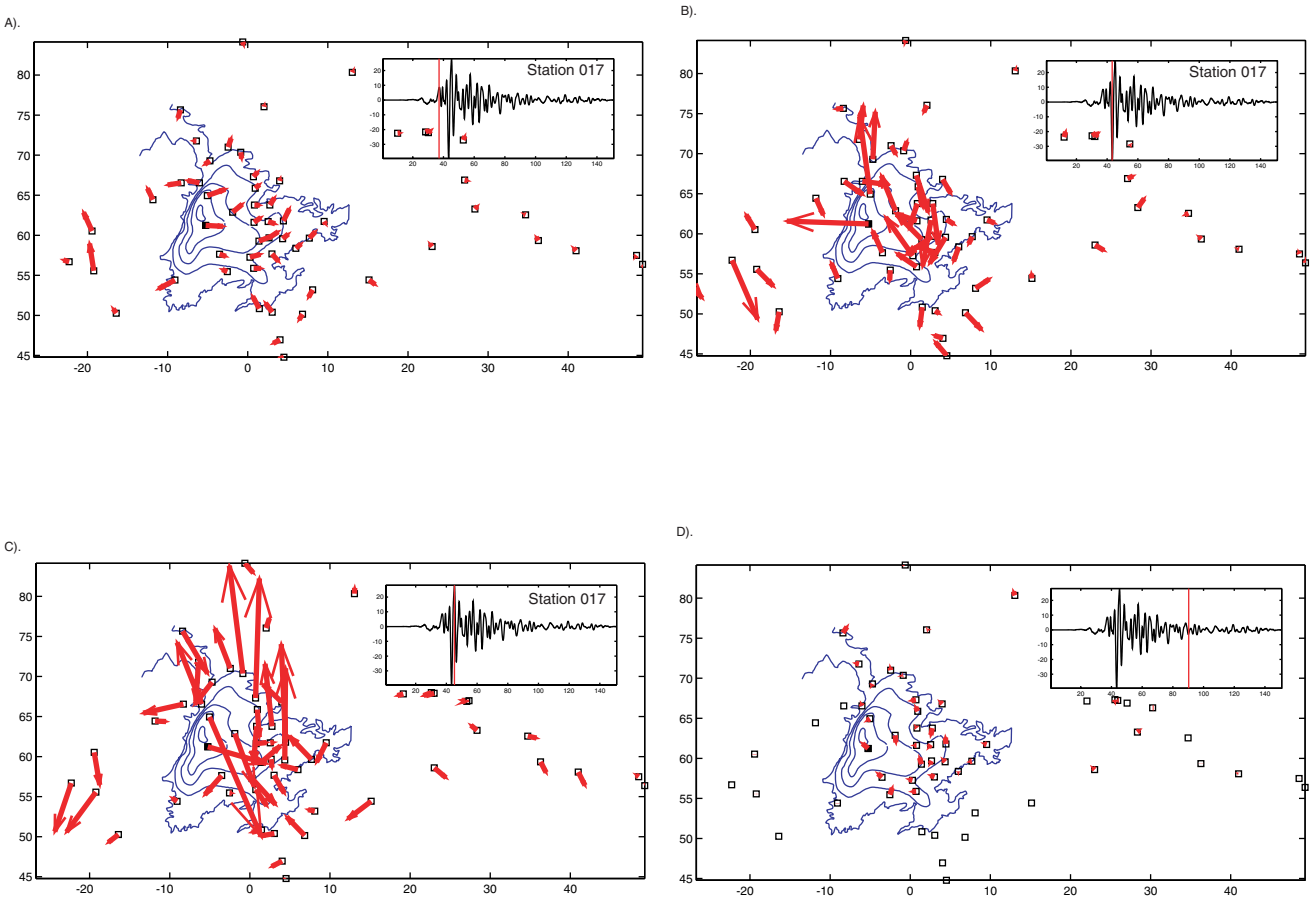

Figure 12. Horizontal polarizations of ground velocity in and near the Taipei basin. Four separate windows are shown: (a) before the main *S*-wave arrival; (b) during an early large peak of the *S* wave (c); another peak just a few seconds later; and (d) about 20 sec later in the coda.

center and opposite to those just across the western edge of the basin. In conclusion, we see strong contrasts in polarity across certain parts of the basin and its boundaries. These opposite polarities would cause large strains and would be important for large extended structures such as bridges.

One of the dominant effects is that the shaking at stations in the basin is higher longer than at stations outside the basin. Figure 12d shows that at 90 sec into the record (using elapsed time at station 017) only basin stations arestill recording with significant ground motion. This could be caused by a difference in triggering parameters, but that so many different stations are behaving in a similar manner suggests trigger settings are not the cause.

Durations

Envelopes of each station in both velocity and acceleration are plotted in Figure 13 along with an average for stations inside and outside the basin. The general amplification at stations in the basin is apparent in these plots as the red curves (basin stations) are above the green curves (from stations outside the basin) until about 50 sec after the largest amplitudes, which are from the Rayleigh wave. Also, duration of records at stations in the Taipei basin are typically longer than those outside the basin. Because scattering would increase the later coda, this observation suggests that the lengthening of the duration of these records is caused by the amplification of ground motion in the basin and not scattering. In Figure 14, the durations of the strong-motion accelerograms are plotted versus depth and a correlation is found with a coefficient of 0.19. In particular, the longest durations are found at the stations over the deepest part of the basin. The similarity of Figure 14 to Figure 5 suggests that the longer duration of records from basin stations is caused by the amplification in low-velocity alluvium in the basin and not scattering.

Coda Q

Nevertheless, Q determined from the coda should provide evidence of the scattering nature of the basin. We use the method of Wong *et al.* (2001) and Pulli (1984), which is based on the single-scattering model and can be used for early coda. The envelope curve is computed as the rms of

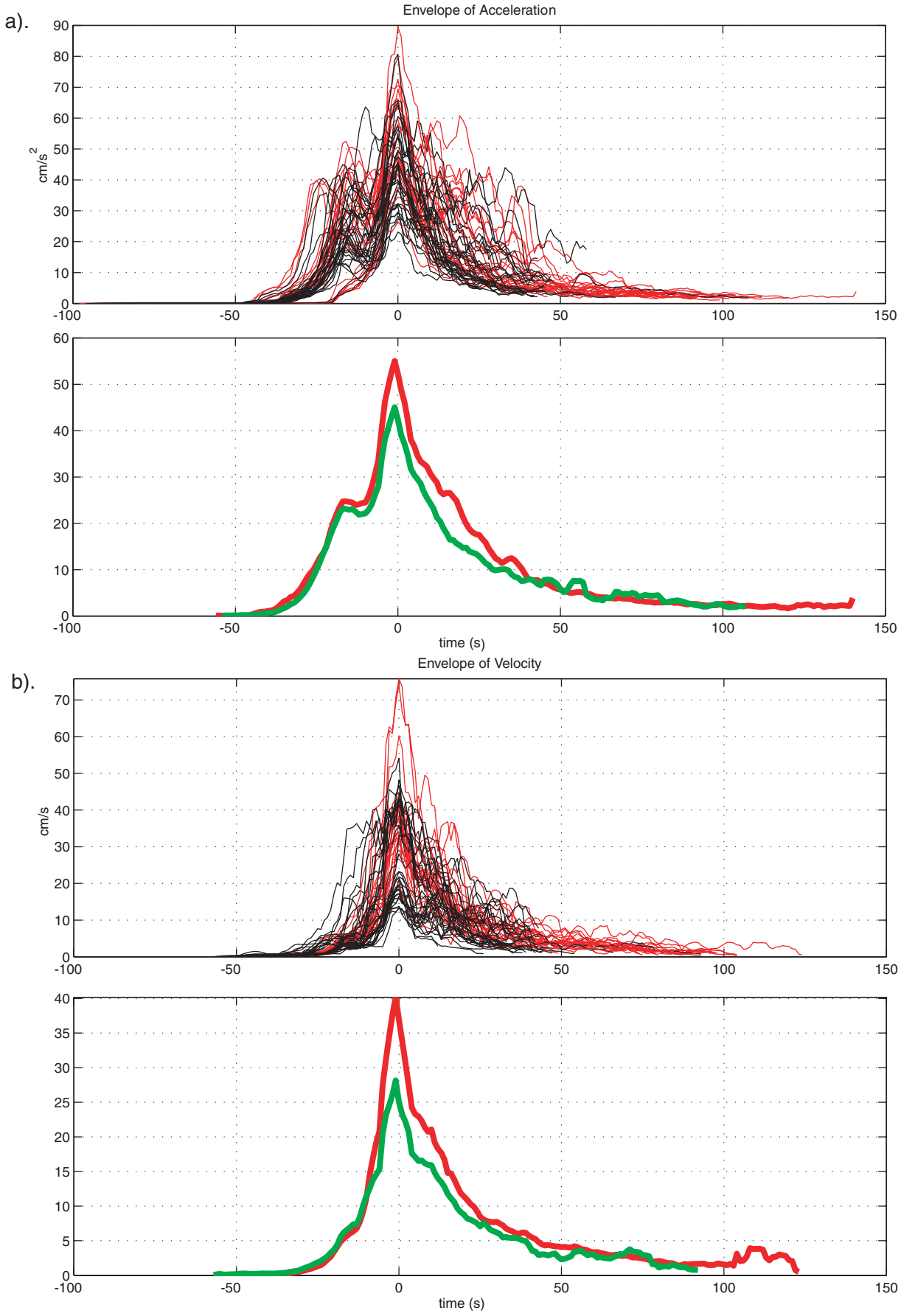

Figure 13. Envelopes of strong ground motion at stations near the Taipei basin (vertical component): (a) Envelope of acceleration. Stations located within the boundary of the Taipei basin are red; outside stations are green. Top plot shows each trace and the bottom plot the averages for each group. (b) Envelope of velocity as in (a). Amplifications near peak (Rayleigh wave) are larger than in (a), but overall envelopes of velocity seem to behave similarly to envelopes of acceleration.

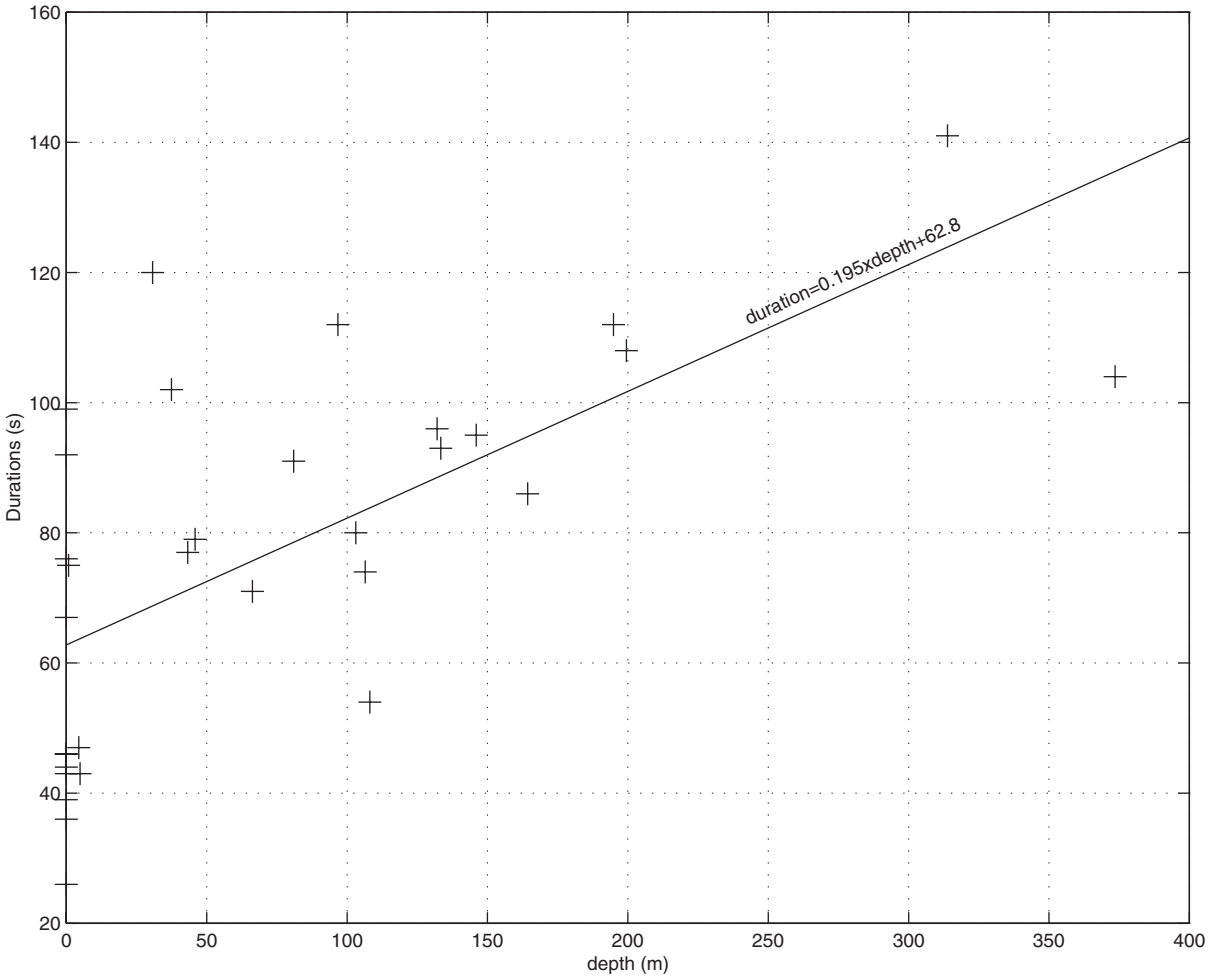

Figure 14. Duration of strong-motion records versus depth to basement. Duration is measured as the length of record after the peak in acceleration records (Rayleigh wave). This assumes there is no systematic difference in the triggering parameters of the accelerographs.

the coda amplitudes after the seismogram has been filtered in a particular frequency band. This envelope curve is then multiplied by the scattering function

$$K(\alpha) = \frac{1}{\alpha} \ln\left[(\alpha+1)\Big/(\alpha-1)\right], \tag{1}$$

where α is t/t_s, t is the elapsed time from the origin time, and t_s is the lapse time of the S wave. Q is determined from the slope of

$$F(t) = \log_{10}[(A_c(t)/A_s)^2 K^{-1}(\alpha)] \tag{2}$$

plotted versus lapse time $t - t_s$. Equation 3 when plotted versus $t - t_s$ has the form

$$F(t) = C(f) - b(t - t_s) \tag{3}$$

and Q is determined from the slope by

$$\mathrm{Q} = \frac{2\pi f \log(e)}{b}. \tag{4}$$

Coda Q for the basin is shown in Figure 15 for a narrow frequency band centered at 1 Hz because this band had the best signal-to-noise ratio. The fit for equation (3) is done for the window 15 to 45 sec after the main arrival (Rayleigh wave). Each value is the average of the Qs from the two horizontals. The values of coda Q are higher in the basin, especially in the eastern end (the shallower end). However, the scatter in values is high, and the average value for stations inside the basin is not significantly greater than for those outside the basin (67 for the sum of eastern stations in the basin compared to 61 outside). This difference is not great enough to cause a major difference in the length of record duration. In conclusion, it appears that amplification of waves caused the lengthening of the strong-motion duration, but scattering in the coda may also play a minor role.

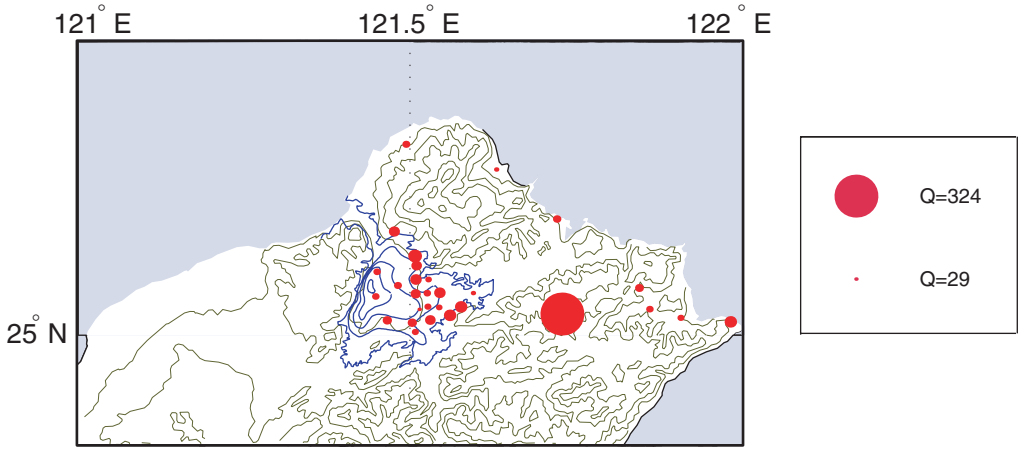

Figure 15. Coda Q for the bandwidth 0.67 to 1.0 Hz for vertical velocity after the arrival of the Rayleigh wave.

Discussion

Wen *et al.* (1995) investigated the effect of the Taipei basin on ground motion from three M 5–6 events that occurred off the northeast coast of Taiwan. They found that peak acceleration did not correlate well with basin depth, but peak velocity did. The largest peak acceleration was concentrated near the edges of the basin. Wen *et al.* (1995) also filtered the acceleration time series to show that at low frequencies (0.1 to 0.8 Hz), peak acceleration behaved in a manner similar to peak velocity, with the largest values near the deepest part of the basin. This result suggests that the tendency for peak acceleration to have the largest values near the edges, but for peak velocity to be associated with the deepest part of the basin, is a robust effect and not dependent on earthquake location. This result is also consistent with spectral ratios (Wen and Peng, 1998) from a set of regional events, which show a greater amplification over the western or deeper part of the basin at periods greater than 1.5 sec, but at higher frequencies, amplifications are spread along the northeast to southeast boundaries (Wen and Peng, 1998).

The dependence of ground motion on basin geometry is an important problem in the Los Angeles region because of the number and depth of basins there, which contribute to an already high seismic hazard. These basins can be as deep as 5 to 6 km. Field (2000) showed that an amplification of about 2 in a 1.0-sec response spectral acceleration should be assigned to the effect of depth in the basins. This factor is the difference for residuals at stations over shallow and deep parts of the basin after applying a model for distance- and magnitude-dependence of strong ground motion (Boore *et al.*, 1997; Field, 2000). In fact, Field (2000) shows (his Fig. 3) residuals for three periods of response spectral acceleration and peak ground acceleration (PGA). The best-fitting slope (peak motion versus depth) for the PGA and 0.3 sec spectral acceleration (SA) is one-half of that for the longer period values of SA (1 and 3 sec). This behavior is consistent with our observation in the Taipei basin that the effect of the basin depth is stronger at longer periods (velocity versus acceleration) than shorter periods. Slopes of amplification in SA or PGA versus depth for the data in the Los Angeles region (Field, 2000) do not predict the amplification values for the Taipei basin, which would be expected considering the large difference in basin depths.

Olsen (2000) modeled wave propagation up to 0.5 sec in the Los Angeles basins using a fourth order staggered-grid, finite-difference scheme. He separated out the effect of the 1D propagation in the low-velocity sediments in the basin from the 3D effect of the geometry of the basin on wave amplitude. He concluded that the mean amplification of the basins (for several scenario events) was about 3.3 for stations over the deepest part, but that a factor of about 2 was caused by the 1D response of the stack of low-velocity layers in the basins (Figures 8 and 9, Olsen, 2000). This is also similar to the results from the Taipei basin in that the 1D response of the basin also introduces significant resonances into the ground motion. Total average amplification in the Taipei basin is about a factor of 40% in acceleration, which is less than that for the examples modeled by Olsen (2000). Wald and Graves (1998) analyzed ground displacement from the Landers earthquake in the Los Angeles basins and found amplifications of 3 to 4 in the Los Angeles but smaller values of about 3 in the San Fernando basin. Again, amplification appears to correlate with depth to basement because contours of amplitude are mostly centered on the basins.

Olsen (2000) also investigated the effect of wave propagation in the Los Angeles basins on the duration of strong ground motion. Although some source locations did not seem to result in a change in the duration of shaking in the basins, among the nine examples he considered, most had dramatically longer duration of shaking in the basins than out. Outside the basins, he found durations as short as 5 sec compared to 45 sec at stations in some of the basins for

simulated events on the Palos Verde fault or the Newport Inglewood fault. For the particular simulation of an event on the San Andreas Fault, the long-period motion in the Los Angeles basin includes surface waves generated at the northern edge of the basins.

Shear-wave polarizations can be a sensitive indicator of refraction around boundaries of low-velocity features. Koketsu and Kikuchi (2000) showed how the polarization of Love waves were bent traversing the edge of the Kanto basin nears the city of Tokyo. In Taipei, the polarizations at stations to the west of the basin are clearly different from polarization directions at stations within the basin. These stations should have about the same hypocentral distance. Apparently wave fronts are bent around this western boundary to the basin, which may be fault-controlled (Bonilla, 1975).

The location of damage in the Taipei basin is shown in Figure 16 to show the relation of damage to basin depth. It is apparent that while one building located over the deep part of the basin collapsed, other heavily damaged buildings are located over shallower parts of the basin. The southeast corner of the basin is, however, a site of higher amplification for periods shorter than 2 sec (Wen and Peng, 1998). Also, amplification has been observed at lower frequencies (<0.5 Hz) at areas where the Sungshan formation seems to be thicker than average. Consequently, understanding the spatial pattern of damage may require better knowledge of formation thickness and geotechnical properties of the sediments in the basin as well as 3D simulation of the propagation of seismic waves through the basin.

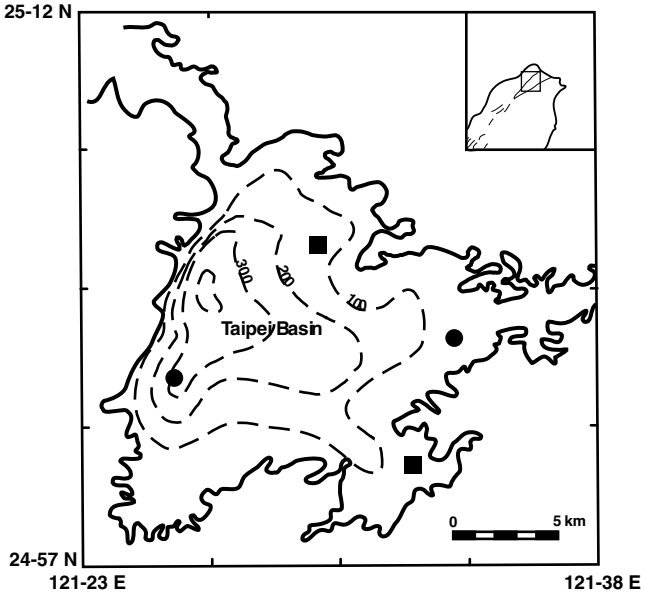

Figure 16. Location of damage to buildings in the Taipei basin from the Chi-Chi earthquake. Circles are buildings with 12 floors and squares are those fewer than 5 floors that were heavily damaged in the earthquake.

Conclusions

Peak accelerations and velocities from the Chi-Chi earthquake are significantly amplified at stations in the Taipei basin compared to other stations in the approximately same distance range. The change is about a 40% increase in peak acceleration and 37% in peak velocity. Peak velocity is well correlated with depth to basement, but peak accelerations are not and may be more influenced by basin-edge effects. Records from basin stations have a high-frequency signal (compared to the main period of the surface wave on the vertical) with frequencies that range from about 0.4 to 1 Hz and are well predicted by 1D models of the response of basin sediments at deeper sections of the basin. The calculated 1D response at stations over shallower sections of the basin does not match well the frequency content of their records of ground motion. Shear-wave polarizations are coherent across the eastern end of the basin, but typically have a strong contrast across the western boundary, suggesting a strong lateral refraction there. Coda durations are longest in the basin, probably caused by the amplified waves there. Coda Qs are only slightly larger at basin stations.

Acknowledgments

We would like to thank W.H.K. Lee for early copies of the strong-motion data set and for many clarifications about the data set afterward. We are thankful for insightful reviews by P. Spudich and J. Andrews.

References

Aki, K., and P. G. Richards (2002). *Quantitative Seismology*, Second Ed., University Science Books, Sauselito, California.

Bonilla, M. G. (1975). A review of recently active faults in Taiwan, *U.S. Geol. Surv. Open-File Rept. 75-41*, 43 pp.

Boore, D. M. (2001). Comparisons of ground motions from the 1999 Chi-Chi earthquake with empirical predictions largely based on data from California, *Bull. Seism. Soc. Am.* **91,** 1212–1217.

Boore, D. M., W. B. Joyner, and T. E. Fumal (1997). Equations for estimating horizontal response spectra and peak acceleration from western North American earthquakes: a summary of recent work, *Seism. Res. Lett.* **68,** 128–153.

Campbell, K. W. (1997). Empirical near-source attenuation relationships for horizontal and vetical components of peak ground acceleration, peak ground velocity, and pseudo-absolute acceleration response spectra, *Seism. Res. Lett.* **68,** 154–179.

Chi, W.-C., D. Dreger, and A. Kaverina (2001). Finite-source modeling of the 1999 Taiwan (Chi-Chi) earthquake derived from a dense strong-motion network, *Bull. Seism. Soc. Am.* **91,** 1144–1157.

Chung, J.-K., and T.-C. Shin (1999). Surface-wave analysis in the Taipei basin from strong-motion data, *TAO*, **10,** 633–650.

Field, E. H. (2000). A modified ground motion attenuation relationship for southern California that accounts for detailed site classification and a basin-depth effect, *Bull. Seism. Soc. Am.* **90,** no. 6b, s209–s221.

Haskell, N. (1953). The dispersion of surface waves on multilayered media, *Bull. Seism. Soc. Am.* **43,** 17–34.

Joyner, W. B., and D. M. Boore (1981). Peak acceleration and velocity from strong-motion records including records from the 1979 Imperial Valley, California, earthquake, *Bull. Seism. Soc. Am.* **71,** 2011–2038.

Joyner, W. B., and D. M. Boore (1988). Measurement, characterization, and prediction of strong ground motion, *Proceedings of Earthquake*

Engineering and Soil Dynamics II, Div/ASCE, Park City, Utah, 43–102.

Joyner, W. B., R. E. Warrick, and A. A. Oliver, III (1976). Analysis of seismograms from a downhole array in sediments near San Francisco Bay, *Bull. Seism. Soc. Am.* **66,** 937–958.

Koketsu, K., and M. Kikuchi (2000). Propagation of seismic ground motion in the Kanto Basin, Japan, *Science*, **288,** 1237–1239.

Lee, W. H. K., T. C. Shin, K. W. Kuo, and K. C. Chen (1999). CWB Free-field strong-motion data from 921 Chi-Chi earthquake Volume 1. Digital acceleration files on CD-ROM, Seismology Center, Central Weather Bureau, Taipei, Taiwan, prepublication version: 6 December 1999.

Lin, S.-B. B., and C.-H. Chen (2001). Geological implications of the sediments from TA-AN No. 1 and the extended Wuku No. 1 boreholes in the Taipei basin, *Western Pacific Earth Sci.* **1,** 473–486.

Olsen, K. B. (2000). Site amplification in the Los Angeles basin from three-dimensional modeling of ground motion, *Bull. Seism. Soc. Am.* **90,** no. 6b, s77–s94.

Pulli, J. J. (1984). Attenuation of coda waves in New England, *Bull. Seism. Soc. Am.* **74,** 1149–1166.

Shin, T.-C., and T.-L. Teng (2001). An overview of the 1999 Chi-Chi, Taiwan, earthquake, *Bull. Seism. Soc. Am.* **91,** 895–913.

Shin, T. C., K. W. Kuo, W. H. K. Lee, T. L. Teng, and Y. B. Tsai (2000). A preliminary report on the 1999 Chi-Chi (Taiwan) earthquake, *Seism. Res. Lett.* **71,** 24–30.

Wald, D. J., and R. W. Graves (1998). The seismic response of the Los Angeles basin, California, *Bull. Seism. Soc. Am.* **88,** 337–356.

Wang, C. Y., Y. H. Lee, and H. C. Chang (1996). *P*- and *S*-velocity structures of the Taipei basin, Symposium on Taiwan Strong-Motion Instrumentation Program (II), Central Weather Bureau, 171–177.

Wen, K.-L., and H.-Y. Peng (1998). Site effect analysis in the Taipei basin: results from TSMIP network data, *TAO* **9,** 691–704.

Wen, K-L., H.-Y. Peng, and L.-F. Liu (1995). Basin effects analysis from a dense strong motion observation network, *Earthquake Eng. Struct. Dyn.* **24,** 1069–1083.

Wong, V., C. J. Rebollar, and L. Munguia (2001). Attenuation of coda waves at the Tres Virgenes Volcanic Area, Baja California Sur, Mexico, *Bull. Seism. Soc. Am.*, **91,** 683–693.

Wu, C., M. Takeo, and S. Ide (2001). Source process of the Chi-Chi earthquake: a joint inversion of strong motion data and global positioning system data with a multifault model, *Bull. Seism. Soc. Am.* **91,** 1128–1143.

Youngs, R. R., S.-J. Chiou, W. J. Silva, and J. R. Humphrey (1997). Strong ground motion attenuation relationships for subduction zone earthquakes, *Seism. Res. Lett.* **68,** 58–73.

U.S. Geological Survey
345 Middlefield Road
Menlo Park, California 94025
(J.B.F.)

Institute of Geophysics
National Central University, Taiwan
(K.-L.W.)

Manuscript received 19 February 2004.